Hindawi
International Journal of Photoenergy
Volume 2018, Article ID 8474017, 12 pages
https://doi.org/10.1155/2018/8474017

Research Article

E. coli Bacteriostatic Action Using TiO_2 Photocatalytic Reactions

Thammasak Rojviroon[1] **and Sanya Sirivithayapakorn**[2]

[1]*Department of Civil Engineering, Faculty of Engineering, Rajamangala University of Technology Thanyaburi, Pathum Thani 12110, Thailand*
[2]*Department of Environmental Engineering, Faculty of Engineering, Kasetsart University, Bangkok 10900, Thailand*

Correspondence should be addressed to Thammasak Rojviroon; thammasak@rmutt.ac.th

Received 12 April 2018; Accepted 3 July 2018; Published 7 August 2018

Academic Editor: Mohammad Al-Amin

This experimental research comparatively investigates the *Escherichia coli (E. coli)* bacterial inactivation of the TiO_2 photocatalytic thin films fabricated by the sol–gel dip-coating (SG) and low-temperature spray-coating (SP) techniques, with low-intensity ($12\,\mu W{\cdot}cm^{-2}$) UVA-light-emitting diodes (UVA-LED) as the light source. The bacteriostatic experiments were undertaken using the nutrient broth (NB) and 0.85% NaCl with the initial *E. coli* concentrations of 10^2, 10^4, 10^6, and 10^8 CFU·mL^{-1}. Moreover, the essential physical characteristics of the SG-TiO_2 and SP-TiO_2 photocatalytic thin films were determined prior to the experimental bacterial inactivation. The findings showed that both photocatalytic thin films possessed the ideal physical characteristics, especially the SP-TiO_2 thin film. In addition, the viable cell counts, the cell morphology, and the bioluminescence-based adenosine triphosphate (ATP) indicated that both SG-TiO_2 and SP-TiO_2 thin films under UVA could effectively inhibit the proliferation of the *E. coli* cells in both NB and 0.85% NaCl.

1. Introduction

The recent decades have witnessed a growing interest in the development of innovative antibacterial technologies against pathogens in the aquatic environment. The phenomenon is attributable to the drawbacks inherent in the existing technologies, including the implementation challenge, the high operation and maintenance costs, and the carcinogenic effects [1–3]. Moreover, the long-term use of antibiotics could cause the bacteria to become antibiotic-resistant and render the drugs less effective in controlling the spread of diseases [4, 5].

One such innovative antibacterial technology is the photocatalytic reactions in the presence of a semiconducting solid catalyst, which generate the free radicals, that is, hydroxyl radicals ($^{\bullet}OH$) and superoxide radicals ($^{\bullet}O_2^-$), which are naturally strong oxidizing agents [6, 7]. In fact, the photocatalytic technology has been utilized in numerous applications, including deodorization, bacterial and viral disinfection, and air and water decontamination [8–11]. The technology is also easy to implement as it essentially requires an ultraviolet light source and a photocatalyst. The most commonly used photocatalyst is titanium dioxide (TiO_2) due to its high levels of photocatalytic activity, prolonged chemical stability, and low toxicity and production cost [12, 13].

Specifically, this experimental research comparatively investigates the TiO_2 photocatalytic thin films fabricated by the sol–gel dip-coating (SG) and low-temperature spray-coating (SP) techniques. In the experiment, the low-intensity UVA-light-emitting diodes (UVA-LED) were used as the light source because they are safer than UVB and UVC, easy to install, inexpensive, lightweight, and energy efficient [14, 15]. Prior to the experimental bacterial inactivation, the essential physical characteristics of the SG-TiO_2 and SP-TiO_2 photocatalytic thin films were determined, including the crystalline phase, bandgap energy, contact angle, morphology, adhesion, and acid-base corrosion resistance.

The experimental bacterial inactivation was carried out using the nutrient broth (NB) and 0.85% NaCl with the initial *E. coli* concentrations of 10^2, 10^4, 10^6, and 10^8 CFU·mL^{-1} treated with the SG- and SP-TiO_2 photocatalytic thin films

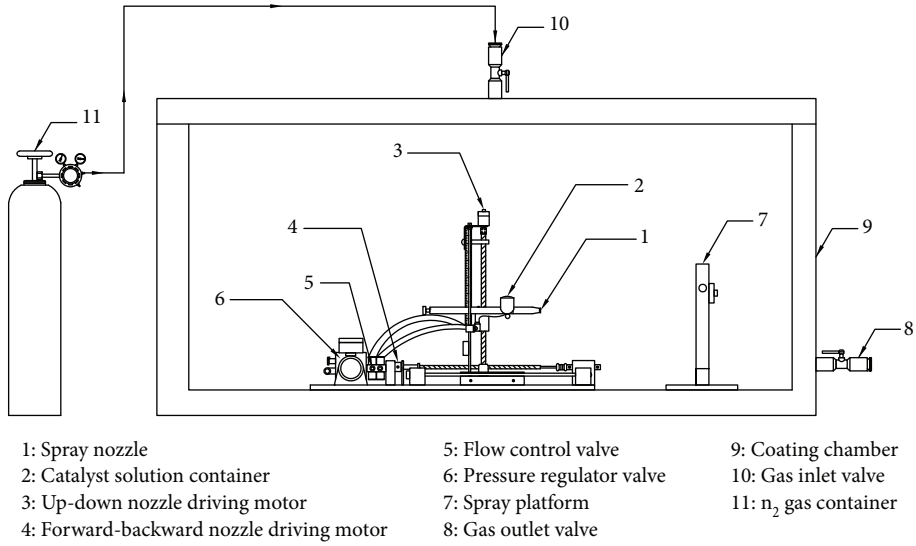

Figure 1: The schematic of the spray-coating chamber.

Table 1: Physical characteristics and the corresponding analysis techniques.

Physical characteristics	Analytical technique/equipment
Crystalline structure	X-ray diffraction/Bruker model D8 Advance
Bandgap energy	Absorption spectrum fitting technique/Thermo Electron's Helios Alpha UV-Vis spectrometer
Contact angle	Sessile drop technique/DataPhysics OCA series TBU90E
Surface morphology	Atomic force microscopy/Asylum Research MFP-3D-BIO
Adhesion test	ASTM method D3359B-17
Corrosion test	Strong acid-base test

and UVA. For comparison, the bacteriostatic activity testing was also conducted in the absence of UVA or the photocatalytic thin films (the control). The bacterial inactivation performance was determined by the viable cell count using the standard plate count (SPC) method and the bioluminescence-based adenosine triphosphate (ATP) test.

2. Experimental

2.1. Preparation of TiO_2 Thin Films. The photocatalytic thin films were fabricated using the sol–gel dip-coating (SG) and low-temperature spray-coating (SP) techniques, whereby the TiO_2 solution was coated onto borosilicate glass slides ($40.0 \times 85.0 \times 0.3$ mm) and petri dishes (100 mm in diameter $\times$ 15 mm in height). The SG- and SP-TiO_2 thin films on the borosilicate glass slides and the petri dishes were for determination of the physical properties and the *E. coli* bacteriostatic action, respectively.

The SG-TiO_2 thin film was prepared using the TiO_2 acid-catalyzed sol–gel dip-coating process [16]. The sol–gel solution was prepared using titanium isopropoxide ($C_{12}H_{28}O_4Ti$, TTIP) and isopropanol (C_3H_7OH) in a volume ratio of 1 : 15 under a pH of 2-3 in a container flushed with N_2 gas at room temperature. The TiO_2 sol–gel solution was then transferred to a container flushed with N_2 gas for dip-coating. In this research, the SG-TiO_2 thin film consisted of five layers of film independently thermally treated: 100°C for the bottom layer and 200, 250, 350, and 500°C for the second, third, fourth, and top layers, respectively.

The low-temperature SP-TiO_2 thin film was produced using the modified TiO_2 composite colloid technique [17]. In the preparation of the TiO_2 composite colloids, 0.01 g of anatase TiO_2 nanoparticles was dispersed in 100 mL of ethanol and polyethylene glycol (PEG) and continuously stirred with a magnetic stirrer at room temperature for 1 hour. The pH of the solution was then adjusted to a pH of 2-3. The colloid solution was then stirred for another 1 hour at room temperature in a container flushed with N_2 and left at room temperature for 24 hours.

The TiO_2 colloid-based photocatalyst was then sprayed onto the substrates (i.e., the glass slide and petri dish) in a proprietary spray-coating chamber (Figure 1). The spray-coating process was carried out at room temperature flushed with N_2. In this research, the SP-TiO_2 thin film was made up of five film layers individually treated at 80°C for 2 hours.

2.2. Physical Characteristics of the SG- and SP-TiO_2 Thin Films. In this research, the crystalline phase of both thin films was analyzed using a D8 Advance X-ray diffractometer

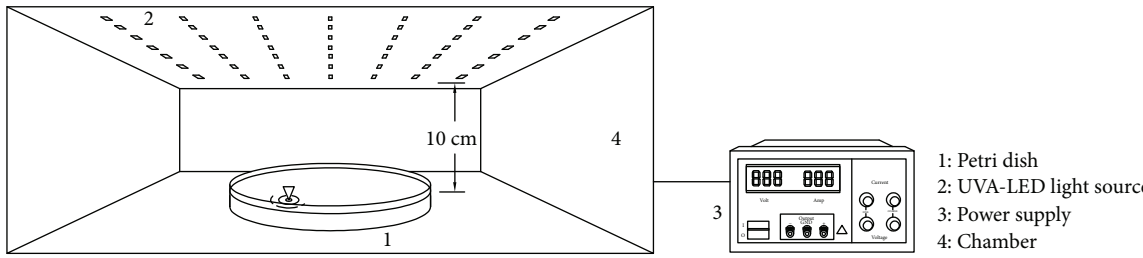

Figure 2: The schematic of the photocatalytic bacterial inactivation system.

(Bruker) under a Cu Kα radiation scan range of 10–80°. The bandgap energy was determined with a Helios Alpha UV-Vis spectrometer (Thermo Electron) with a wavelength range of 290–800 nm. The surface morphology of both SG- and SP-TiO_2 thin films was determined using an MFP-3D-BIO™ Atomic Force Microscope (AFM Asylum Research), and the contact angles were obtained by the sessile drop technique using an OCA series TBU90E instrument (DataPhysics). Specifically, the contact angles were the averages of five replications after reposing a 1 mL water droplet on the experimental thin films for 30 seconds.

The AFM images were analyzed by Gwyddion v.2.22 (http://gwyddion.net) for the grain size and the apparent surface area of the thin films. The adhesion between the thin film and the substrate (i.e., the glass slide) was evaluated in accordance with the ASTM D3359B-17 standard. The acid-base corrosion resistance of the experimental thin films was determined by dipping the coated substrates (i.e., the glass slides with the TiO_2 thin film) for 5 minutes independently in 1 M nitric acid and 1 M sodium hydroxide solution [12, 18]. Table 1 tabulates the physical characteristics of interest and the corresponding analysis techniques.

2.3. Photocatalytic Bacterial Inactivation. Gram-negative bacteria *E. coli* (strain TISTR 073) were used to evaluate the photocatalytic bacterial inactivation of both the SG- and SP-TiO_2 thin films. The stock *E. coli* in −80°C was inoculated into 10 mL brain heart infusion (BHI) broth and incubated at 37°C for 24 h. The product was then inoculated into 30 mL nutrient broth (NB) that contained 3 g beef extract, 5 g peptone, and 1000 mL distilled water and incubated at 37°C (i.e., the substrate enrichment condition) for the initial *E. coli* concentrations (N_0) of 10^2, 10^4, 10^6, and 10^8 CFU·mL^{-1} (*E. coli* in NB).

The procedure was repeated for another batch of the products with the *E. coli* concentrations of 10^2, 10^4, 10^6, and 10^8 CFU·mL^{-1} prior to centrifugation at 3000 rpm for 10 min at room temperature. The supernatant was discarded, and the subnatant (i.e., the *E. coli* cells) was harvested and washed three times with 0.85% NaCl. The bacterial cells were then resuspended in 30 mL 0.85% NaCl (i.e., the nonsubstrate enrichment condition) for the initial *E. coli* concentrations in 0.85% NaCl of 10^2, 10^4, 10^6, and 10^8 CFU·mL^{-1} (*E. coli* in 0.85% NaCl).

Afterward, 30 mL aliquots of the NB and 0.85% NaCl with the *E. coli* concentrations of 10^2, 10^4, 10^6, and 10^8 CFU·mL^{-1} were transferred to the petri dishes coated with the SG-TiO_2 or SP-TiO_2 thin film and placed under the UVA light source (warm white UVA-LED) in a photoreactor for 180 minutes (Figure 2). The electric power was controlled by a 12 V 3 A power supply AC-DC adapter. The average UVA intensity in the photoreactor was 12 μW·cm^{-2} such that the energy falling onto the coating surface in an hour was about 1.2 W·h, measured by the UV Light Meter Model UV-340. In this experimental condition, the cool down was not necessary because the average temperature of the photoreactor increased slightly by 1–3°C. The samples were collected after 30, 60, 120, and 180 minutes to analyze the viable cells using the standard plate count (SPC) method. Prior to the viable cell count, a serial dilution was carried out by introducing 1 mL of each sample into 30 mL of 0.85% NaCl. Then 0.1 mL of the serial dilutions was transferred to the plate count agar (PCA) and incubated 24–48 hours at 37°C. The viable cells of *E. coli* were subsequently counted.

Moreover, the viable *E. coli* cells in NB and in 0.85% NaCl (with the initial bacterial concentrations of 10^2, 10^4, 10^6, and 10^8 CFU·mL^{-1}) treated with the SG- and SP-TiO_2 thin films and UVA were verified against the viable cell counts of the control with the identical initial *E. coli* concentrations (i.e., those treated with the thin films in the absence of UVA (dark) and those treated with UVA without the thin films). Figure 3 illustrates the overall scheme of this experimental research.

To further verify the photocatalytic bacterial inactivation performance of both thin films, the ATP bioluminescence assay was carried out for the adenosine triphosphate (ATP). The viable *E. coli* cells were determined by the cellular ATP content using the Lumitester PD-20 (Kikkoman Biochemifa, Japan), based on the detection of light generated by the ATP-dependent enzymatic conversion. Specifically, D-luciferin in the ATP was transformed into oxyluciferin by luciferase whereby the light was generated. The quantity of light emission was measured by the Lumitester and the result expressed as the relative light unit (RLU). The ATP of the viable *E. coli* cells (in RLU) was the averages of five replications of the *E. coli* cells in NB and in 0.85% NaCl, given the initial bacterial concentrations of 10^2, 10^4, 10^6, and 10^8 CFU·mL^{-1}, after 30, 60, 120, and 180 minutes.

3. Results and Discussion

3.1. Physical Characteristics of the Photocatalytic Thin Films. Figure 4 illustrates the X-ray diffraction (XRD) patterns of both experimental thin films, with the peak at the diffraction angle (2θ) of 25.0°. In addition, the analysis results revealed

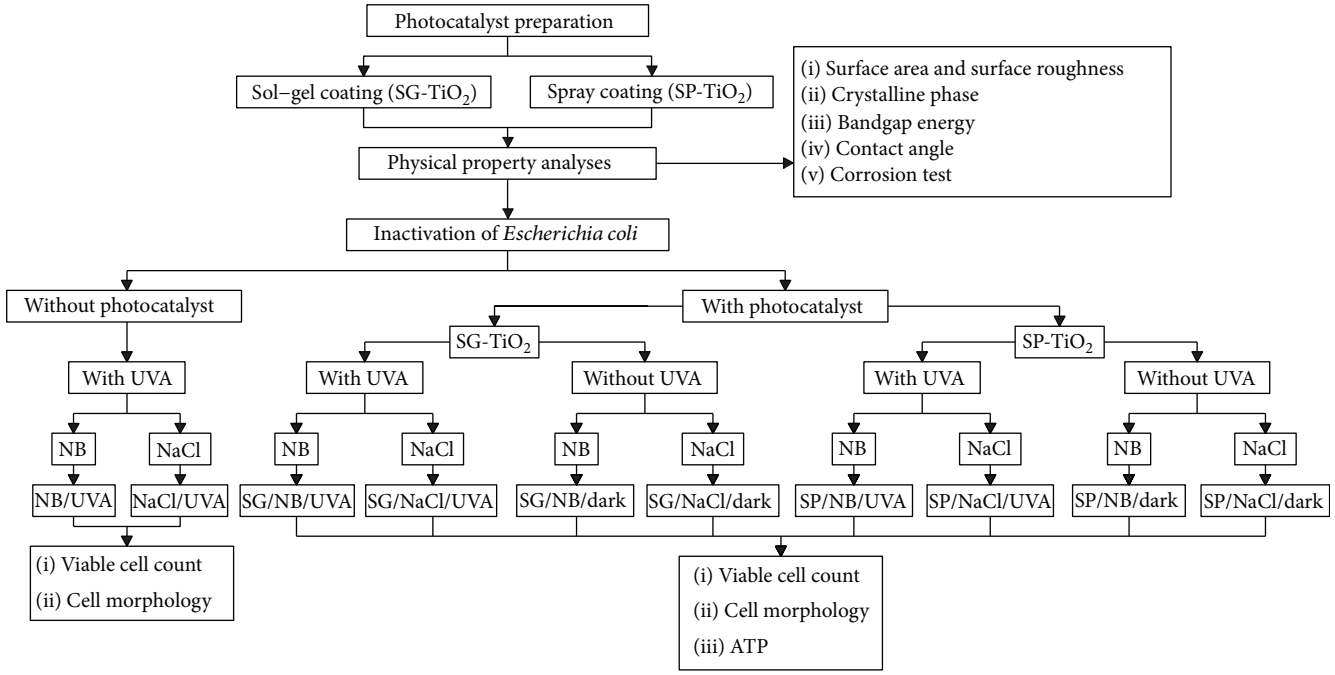

Figure 3: The overall scheme of this experimental research.

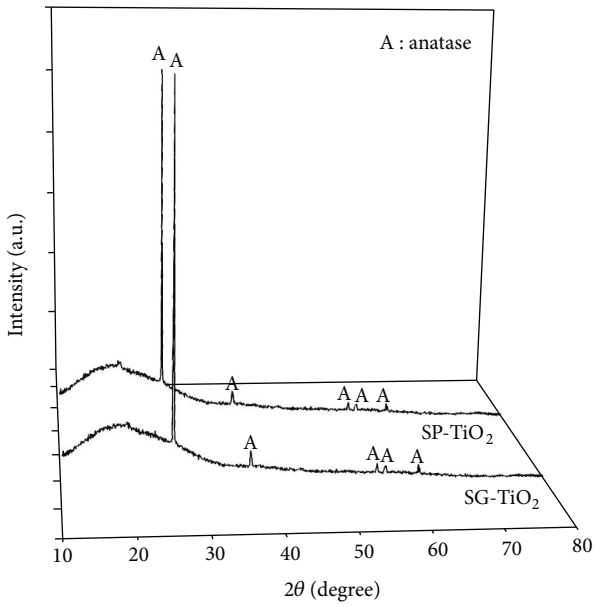

Figure 4: XRD patterns of the SG-TiO_2 and SP-TiO_2 thin films.

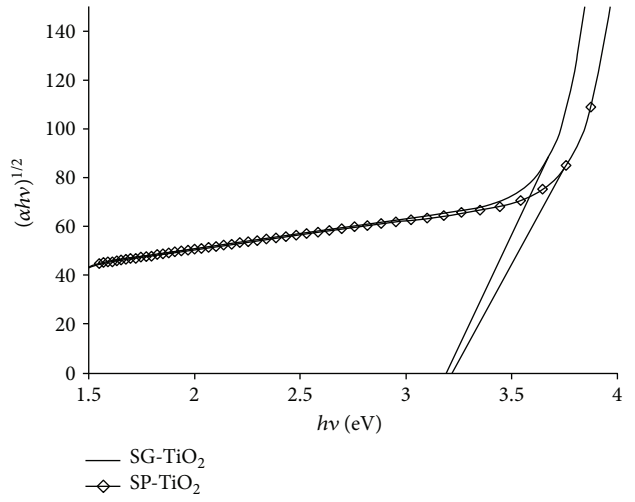

Figure 5: The energy bandgaps of the SG-TiO_2 and SP-TiO_2 thin films.

that only the anatase (101) phase (anatase TiO_2, ICSD code: 01-089-4921) was present (no rutile phase) in both thin films.

The bandgap energy (E_g) is calculated from the linear relationship of $(h\nu\alpha)^{1/2}$ against $h\nu$ with extrapolation to zero, which is referred to as the Tauc plot and can be expressed as [13, 19], where h is Plank's constant (eV), ν is the frequency of vibration, α is the absorption coefficient, A is a proportional constant, and E_g is the bandgap energy (eV).

$$(h\nu\alpha)^{1/2} = A\left(h\nu - E_g\right). \quad (1)$$

Figure 5 illustrates the Tauc plots of both experimental thin films, in which the dotted lines intercepted the x-axis ($h\nu$-intercept) at 3.19 and 3.22 eV for the SG-TiO_2 and SP-TiO_2 thin films, respectively. The findings indicated that the bandgap energies of both thin films were in the range of anatase TiO_2 [20, 21].

In Figure 6, the contact angles of the water droplet on the surface of the SG- and SP-TiO_2 thin films were 46.78° and 57.31°, indicating that both films were hydrophilic [22, 23]. Figures 7(a) and 7(b), respectively, depict the 2D and 3D AFM images of the SG- and SP-TiO_2 thin films, in which the TiO_2 particles were round and uniform and evenly distributed with the grain sizes of 35–90 nm and 25–80 nm

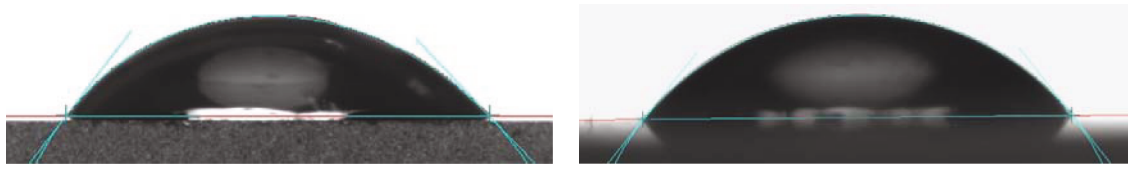

(a) (b)

Figure 6: The contact angles of (a) SG-TiO_2 and (b) SP-TiO_2 thin films.

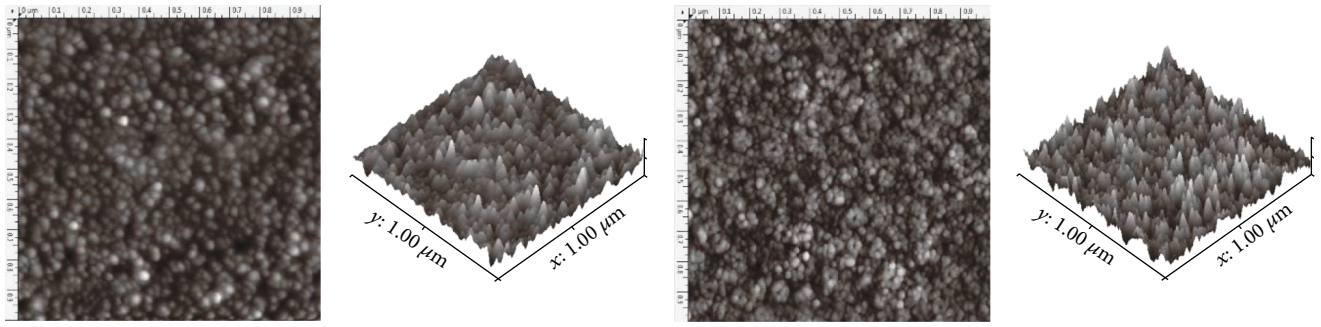

(a) (b)

Figure 7: The 2D and 3D AFM images of (a) SG-TiO_2 and (b) SP-TiO_2 thin films.

Table 2: Physical properties of the SG-TiO_2 and SP-TiO_2 photocatalytic thin films.

Physical properties	Thin films	
	SG-TiO_2	SP-TiO_2
Crystalline phase	Anatase	Anatase
Bandgap energy (eV)	3.19	3.22
Contact angle (°)	46.78	57.31
Measured by Gwyddion analysis		
Grain size (nm)	35–90	25–80
RMS average roughness (nm)	1.75	0.88
Apparent surface area ($m^2 \cdot m^{-2}$) ❶	1.02	1.01
Total weight of TiO_2 on substrate ($g \cdot m^{-2}$) ❷	0.45	0.38
Total apparent surface area per total weight of TiO_2 ($m^2 \cdot g^{-1}$) ❸ = ❶/❷	2.27	2.53
Adhesion		
Rank	Good	
Classification	4B	
Corrosion test	No visible damage	

for the SG- and SP-TiO_2 thin films. The root mean square (RMS) averages of the roughness of the SG- and SP-TiO_2 thin films were 1.75 and 0.88 nm, respectively, resulting in the smooth surface and elevated hydrophilicity, which in turn contributed to the reduced contact angle and increased polar interaction with the water droplet [24].

The hydrophilicity of both thin films transformed the oxidation state from Ti^{4+} to Ti^{3+}, while the photogenerated holes oxidized the O^{2-} anions to O_2. The expulsion of oxygen anions from Ti^{3+} generated $^{\bullet}OH$ and $^{\bullet}O_2^-$ and produced holes which play a crucial role in the photocatalytic activity and bacterial inactivation. In fact, the hydrophilicity, as expressed by the contact angle, could be used to approximate the photocatalytic performance of the TiO_2 thin films [25–27].

In Table 2, the total apparent surface areas per total weight of catalyst of the SG- and SP-TiO_2 thin films were 2.27 and 2.53 $m^2 \cdot g^{-1}$, respectively, indicating that the proposed low-temperature spray-coating (SP) technique increased the total apparent surface area. In addition, both thin films exhibited a good substrate adhesion, achieving the 4B classification. For the acid-base corrosion resistance, neither of the thin films showed visible damage, suggesting a high acid-base resistance.

Table 3 compares the physical characteristics of the SG- and SP-TiO_2 photocatalytic thin films with those of existing research studies using variable coating techniques. Unlike the other techniques whose curing temperatures were in the range of 250 to 500°C, the curing temperature of the SP-TiO_2 thin film of this research was only 80°C. Notably, the SP-TiO_2 thin film possessed the physical characteristics resembling those fabricated under the high temperature conditions. In addition, the low-temperature spray-coating technique requires smaller amounts of TiO_2 and is applicable to the substrates with low thermal resistance. The proposed spray-coating scheme could also be applied to materials with large surface areas at minimal costs and short fabrication time.

3.2. Photocatalytic Bacterial Inactivation. The photocatalytic bacterial inactivation experiments were performed with four initial *E. coli* concentrations in NB and 0.85% NaCl of approximately 10^2, 10^4, 10^6, and 10^8 CFU·mL^{-1}. The SPC was used to quantify the viable cells under the substrate enrichment condition (in NB) and the nonsubstrate

Table 3: Comparison of the properties of the SG- and SP-TiO_2 photocatalytic thin films and of other studies.

Substrate	Catalyst	Amount of Ag (% wt)	Preparation		% crystalline		Bandgap energy (eV)	Contact angle (°)	Number of coating layers	Grain size (nm)	Roughness RMS (nm)	Surface area/weight of catalyst ($m^2 \cdot g^{-1}$)	Reference
			Method	Temp (°C)	Anatase	Rutile							
Glass	SG-TiO_2	—	Sol–gel	500	100	0	3.19	46.78	5	35–90	1.75	2.27*	This study
Glass	SP-TiO_2	—	Spray	80	100	0	3.22	57.31	5	25–80	0.88	2.53*	This study
Glass	TiO_2	—	Spin	500	100	0	—	2	—	50–100	—	—	[28]
Silicon wafer	TiO_2	—	Spin	500	100	0	—	25	3	30	3.44	—	[29]
Glass	TiO_2	—	Sol–gel	500	100	0	3.27	—	5	15–100	2.62–5.74	2.58–10.27*	[30]
Glass	TiO_2	—	Sputtering	250	100	0	3.75	—	—	185	6.87	—	[31]

*The apparent surface area is measured by AFM.

Table 4: *E. coli* inactivation performance of the SG- and SP-TiO_2 thin films under UVA after 180 minutes given the various initial bacterial concentrations.

Initial bacterial concentration of *E. coli* (CFU·mL^{-1})	*E. coli* inactivation ± SD (%) at 180 min with $n = 5$ (number of replication)			
	SG/NB/UVA	SG/NaCl/UVA	SP/NB/UVA	SP/NaCl/UVA
10^2	86.18 ± 1.43	92.53 ± 1.58	84.46 ± 1.67	92.94 ± 1.38
10^4	74.80 ± 1.39	80.77 ± 1.33	72.31 ± 1.69	78.67 ± 1.66
10^6	65.14 ± 1.25	72.40 ± 0.60	65.20 ± 1.55	71.43 ± 1.71
10^8	44.59 ± 1.59	63.72 ± 2.01	47.25 ± 1.98	60.71 ± 2.05

enrichment condition (in 0.85% NaCl). For comparison, this research also determined the viable cell counts of the *control*, given the same initial *E. coli* concentrations (i.e., those treated with the thin films in the absence of UVA (dark) and those treated with UVA without the thin films).

Table 4 compares the *E. coli* inactivation performance of the SG- and SP-TiO_2 photocatalytic thin films under the UVA light, given the initial bacterial concentrations in NB and 0.85% NaCl of 10^2, 10^4, 10^6, and 10^8 CFU·mL^{-1}. The results revealed that the thin-film type (SG- or SP-TiO_2 thin film) had no significant impact on the bacterial inactivation performance. In addition, given the same *E. coli* concentration, the photocatalytic bacterial inactivation in 0.85% NaCl was higher than in NB because the 0.85% NaCl solution was unconducive to the bacterial proliferation. Nevertheless, both experimental thin films under the UVA light were effective in inhibiting the proliferation of the *E. coli* cells in NB (10^2, 10^4, 10^6, and 10^8 CFU·mL^{-1}).

Figures 8(a) and 8(b) illustrate the photocatalytic bacterial inactivation of the SG-TiO_2 thin film under UVA (SG/NB/UVA and SG/NaCl/UVA) relative to that of the control (SG/NB/dark, NB/UVA, SG/NaCl/dark, and NaCl/UVA), given the initial *E. coli* concentrations in NB and 0.85% NaCl of 10^2, 10^4, 10^6, and 10^8 CFU·mL^{-1}. Meanwhile, Figures 8(c) and 8(d) depict the bacteriostatic activity of the SP-TiO_2 thin film under UVA (SP/NB/UVA and SP/NaCl/UVA) vis-à-vis that of the control (SP/NB/dark, NB/UVA, SP/NaCl/dark, and NaCl/UVA), given the same initial *E. coli* concentrations.

The results revealed that both SG- and SP-TiO_2 thin films, with the UVA exposure, were able to inhibit the proliferation of *E. coli* under the substrate enrichment (NB) and nonsubstrate enrichment (0.85% NaCl) conditions. Specifically, in the absence of the UVA light or the photocatalytic thin films (SG/NB/dark, SG/NaCl/dark, SP/NB/dark, SP/NaCl/dark, NB/UVA, and NaCl/UVA), the *E. coli* growth was normal. On the other hand, with the UVA exposure and the thin films (SG/NB/UVA, SG/NaCl/UVA, SP/NB/UVA, and SP/NaCl/UVA), the bacterial abundance declined. The reduction in the *E. coli* cells indicated that both photocatalytic thin films, given the UVA exposure, could effectively inhibit the bacterial growth. In addition, the photocatalytic bacterial inactivation performance increased with the elongated UVA irradiation time.

The bacterial inactivation analysis revealed that neither TiO_2 nor UVA could independently inhibit the growth of *E. coli*. In fact, the concurrent deployment of the photocatalytic thin film (SG- or SP-TiO_2 thin film) and the UVA light source is imperative to induce the bacteriostatic activity of the *E. coli* cells. The results showed that both thin films were good enough to inhibit the growth of *E. coli* cells (bacteriostatic) but not kill them (bactericidal). Since this prepared photocatalyst can be applied onto different surfaces, there are potential applications for surfaces that are needed to control the proliferation of bacteria, such as a kitchen counter, inside surface of a refrigerator, and door knobs, in order to gain benefit through a more eco- and environment-friendly process when compared to the use of harmful chemicals.

Figure 8 indicates the abundance of $^{\bullet}OH$ species [32, 33]. $^{\bullet}OH$ is bacteriostatic or even bactericidal and is an oxidizing agent stronger than chlorine, hydrogen peroxide, or even ozone [18, 34–36]. $^{\bullet}OH$ is generated as the holes in the valence band oxidize H_2O molecules to generate $^{\bullet}OH$ for the oxidation pathway and O_2 captures the electrons in the conduction band to produce $^{\bullet}O_2^-$ and subsequently generate $^{\bullet}OH$ for the reduction pathway [32, 33]. The high photocatalytic bacteriostatic action was attributable to the oxidation of *E. coli* by $^{\bullet}OH$ and $^{\bullet}O_2^-$. In Figure 8, the reaction kinetics of photocatalytic bacterial inactivation under a UVA-LED light can be described by pseudo first-order kinetics, and the highest kinetics constants for *E. coli* concentrations in NB and 0.85% NaCl of 10^2 CFU·mL^{-1} were 4.5×10^{-3} and 5.8×10^{-3} min^{-1} for the SG-TiO_2 thin film, respectively, and were 4.1×10^{-3} and 6.0×10^{-3} min^{-1} for the SP-TiO_2 thin film, respectively.

Moreover, the bacteriostatic activity was further verified with the FE-SEM images of the *E. coli* cells, in addition to the SPC method. Figures 9(a)–9(d) illustrate the morphology and structure of the *E. coli* cells in NB and 0.85% NaCl after 180 minutes (at termination) treated with the SG- and SP-TiO_2 thin films and UVA irradiation, given the initial bacterial concentration of 10^4 CFU·mL^{-1}, vis-à-vis the control (Figure 9(e)). The FE-SEM images showed that, with the photocatalytic thin films and UVA, the outer cell membranes exhibited the deformation or even destruction (Figures 9(a)–9(d)).

In Figures 9(a)–9(d), the *E. coli* cells were mostly either irreversibly deformed or collapsed, with fissures and pits visible on the cell membrane, indicating the loss of integrity and viability of the *E. coli* cells, consistent with [37–40]. In fact, the bacterial inhibition performance of the SG-TiO_2 thin film, given the UVA exposure, resembles that of the SP-TiO_2 thin film. The similarity could be attributed to the similar total apparent surface areas of the SG-TiO_2 (2.27 m^2·g^{-1}) and SP-TiO_2 (2.53 m^2·g^{-1}) thin films.

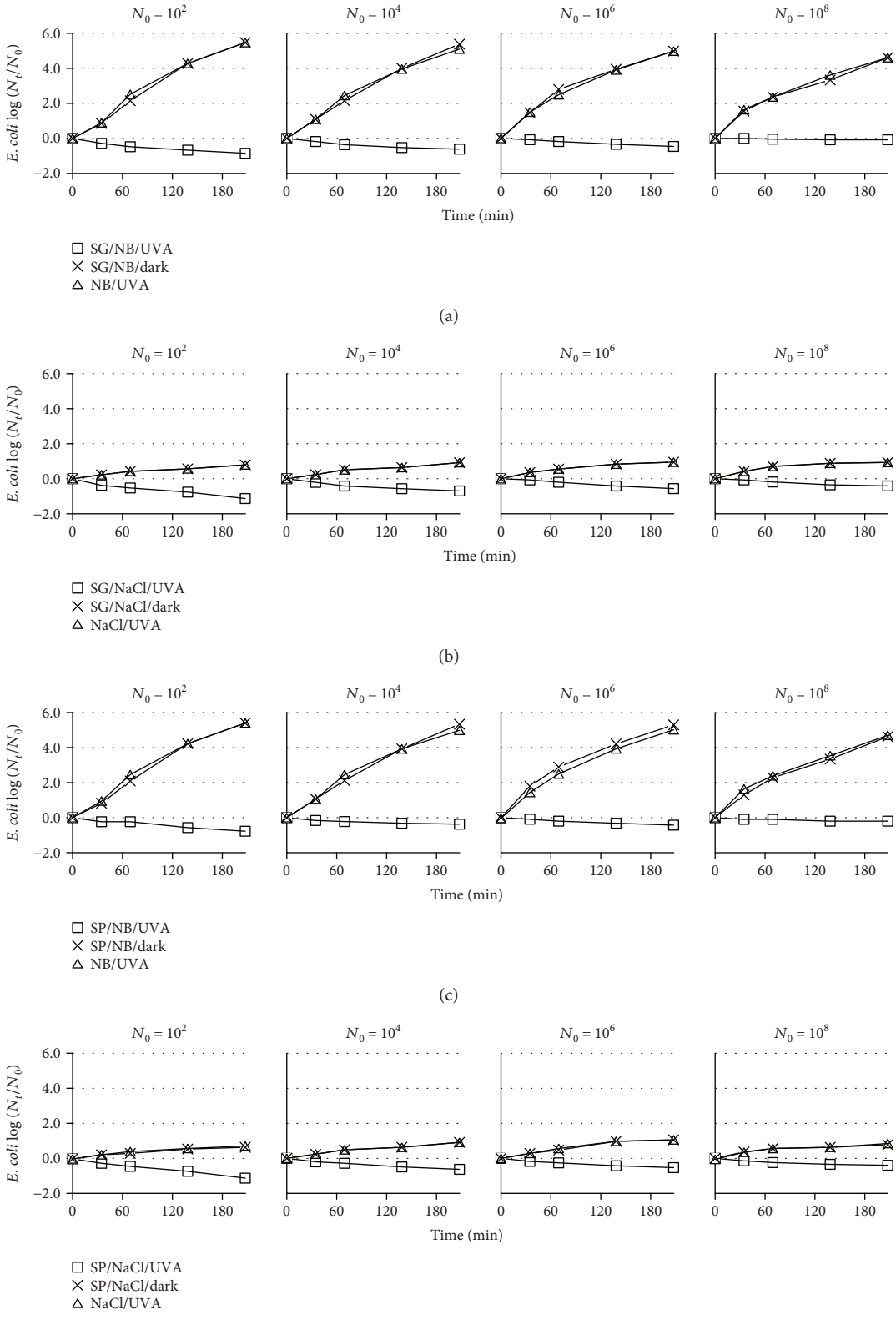

Figure 8: The photocatalytic bacterial inactivation, given the initial *E. coli* concentrations in NB and 0.85% NaCl of 10^2, 10^4, 10^6, and 10^8 CFU·mL^{-1}: (a) NB treated with SG-TiO_2 thin film and UVA relative to the control (SG/NB/dark and NB/UVA), (b) NaCl treated with SG-TiO_2 thin film and UVA relative to the control (SG/NaCl/dark and NaCl/UVA), (c) NB treated with SP-TiO_2 thin film and UVA relative to the control (SP/NB/dark and NB/UVA), and (d) NaCl treated with SP-TiO_2 thin film and UVA relative to the control (SP/NaCl/dark and NaCl/UVA).

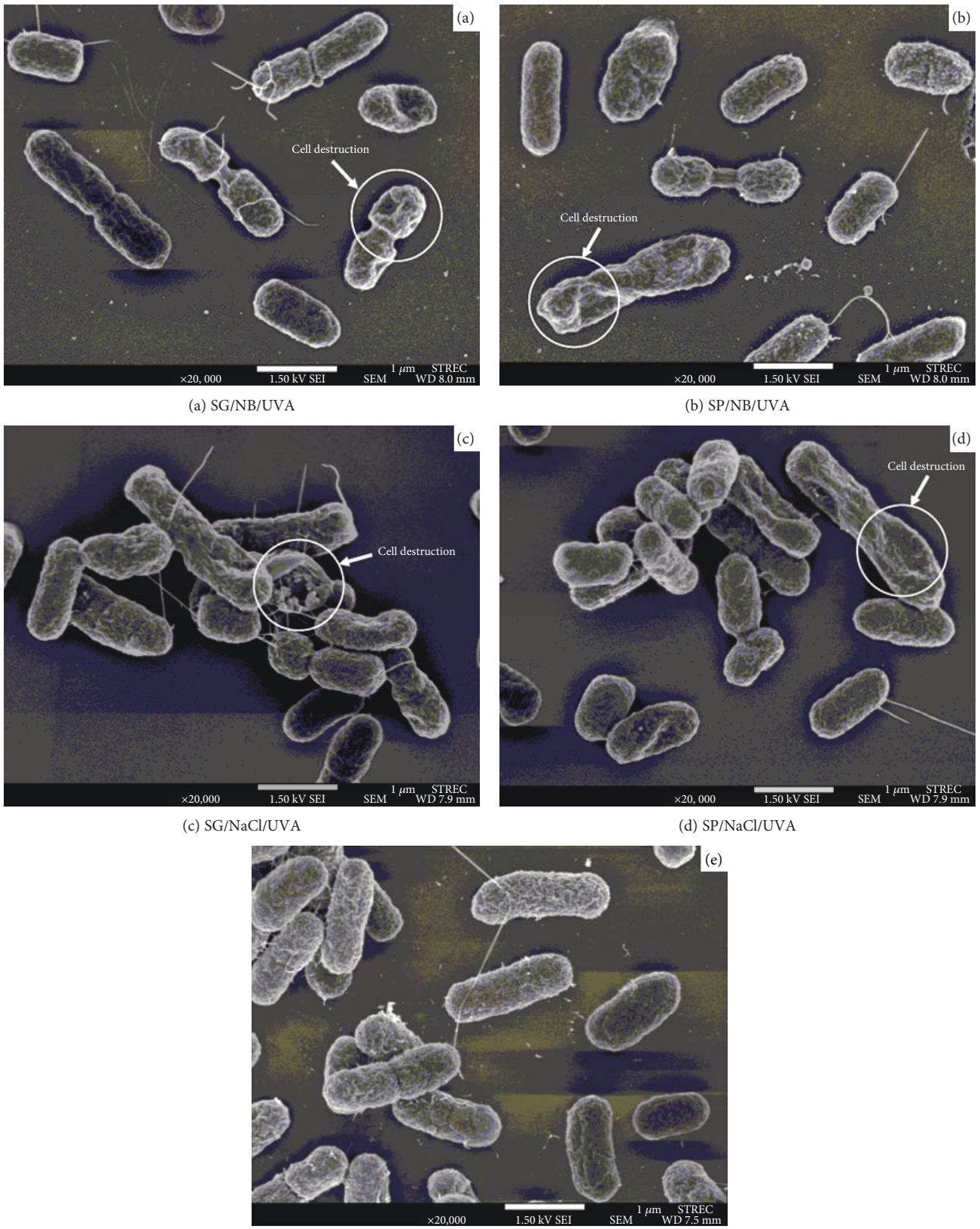

(a) SG/NB/UVA

(b) SP/NB/UVA

(c) SG/NaCl/UVA

(d) SP/NaCl/UVA

(e) Control experiment with only UVA

Figure 9: The FE-SEM images of *E. coli* in NB and 0.85% NaCl after 180 minutes treated with the SG- and SP-TiO_2 thin films and UVA irradiation vis-à-vis the control, given the initial bacterial concentration of 10^4 CFU·mL^{-1}.

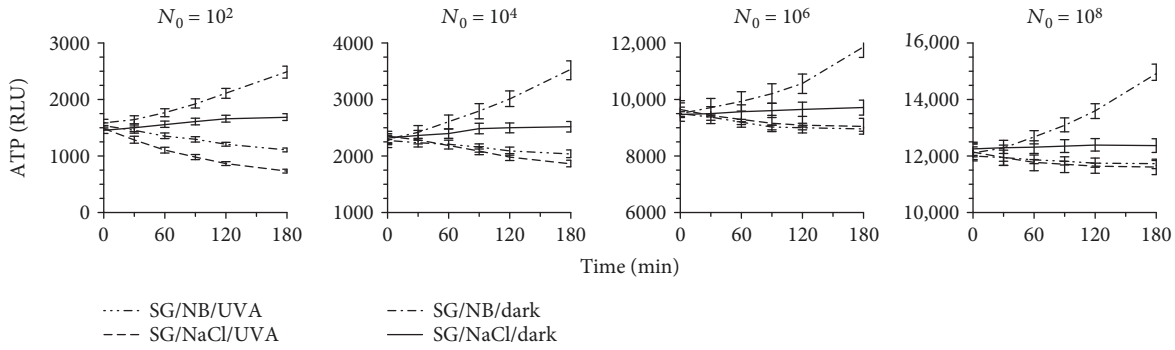

(a) ATP of *E. coli* cells in the NB and 0.85% NaCl treated with the SG-TiO_2 thin film and with or without UVA

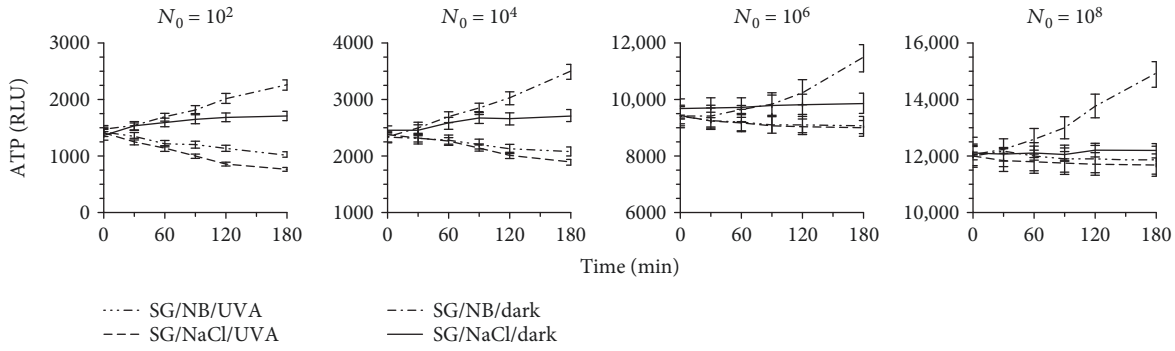

(b) ATP of *E. coli* cells in the NB and 0.85% NaCl treated with the SP-TiO_2 thin film and with or without UVA

Figure 10: The ATP of *E. coli* cells treated with the experimental thin films and with/without UVA.

In Figure 10, the ATP of the *E. coli* cells treated with the SG- and SP-TiO_2 thin films, with and without UVA, validated the SPC results and the bacteriostatic activity. Specifically, the ATP declined as the viable cells decreased, which subsequently led to the decline in the cellular metabolic rates and the eventual cell death.

In short, the concurrent use of the SG- or SP-TiO_2 thin film and UVA could effectively inhibit the proliferation of the *E. coli* cells in both NB and 0.85% NaCl. However, the elevated initial *E. coli* concentrations in NB and 0.85% NaCl lowered the photocatalytic bacterial inactivation performance, due to the restricted active photocatalytic surface site [41–43] and the subsequently lower $^{\bullet}OH$ and $^{\bullet}O_2^-$ [9, 44, 45].

4. Conclusion

The aim of this experimental research is to comparatively examine the *E. coli* bacterial inactivation of the SG-TiO_2 and SP-TiO_2 photocatalytic thin films under the low-intensity UVA light source. The bacteriostatic experiments were undertaken using the NB and 0.85% NaCl with the initial *E. coli* concentrations of 10^2, 10^4, 10^6, and 10^8 CFU·mL^{-1}. The bacteriostatic activity assessments were also carried out without UVA or the photocatalytic thin films (the control). The experimental results revealed that both SG-TiO_2 and SP-TiO_2 photocatalytic thin films possessed the ideal physical characteristics, especially the SP-TiO_2 thin film given its lower fabrication temperature (80°C), subsequent lower energy demand, minimal TiO_2 requirement, and applicability to large surface area objects. In addition, both photocatalytic thin films could effectively inhibit the proliferation of *E. coli* under the low-intensity UVA irradiation, as evidenced by the lower viable cell counts. The bacterial inactivation performance was further verified by the FE-SEM images of deformed *E. coli* cells and the ATP measurement. Nevertheless, the *E. coli* inactivation efficiencies declined as the initial bacterial concentration increased due to the restricted active photocatalytic surface site and the subsequently lower $^{\bullet}OH$ and $^{\bullet}O_2^-$.

Data Availability

The data used to support the findings of this study are available from the corresponding author upon request.

Conflicts of Interest

The authors declare that they have no conflicts of interest.

Acknowledgments

The authors would like to express their deep gratitude to the Thailand Research Fund for TRF Grant for New Researcher (2014): TRG 57802545, and to Rajamangala University of Technology Thanyaburi for the technical assistance.

References

[1] L. B. B. Ndong, M. P. Ibondou, Z. Miao et al., "Efficient dechlorination of chlorinated solvent pollutants under UV irradiation by using the synthesized TiO_2 nano-sheets in aqueous

phase," *Journal of Environmental Sciences*, vol. 26, no. 5, pp. 1188–1194, 2014.

[2] F.-X. Tian, B. Xu, Y.-L. Lin et al., "Chlor(am)ination of iopamidol: kinetics, pathways and disinfection by-products formation," *Chemosphere*, vol. 184, pp. 489–497, 2017.

[3] C. Kolb, R. A. Francis, and J. M. VanBriesen, "Disinfection byproduct regulatory compliance surrogates and bromide-associated risk," *Journal of Environmental Sciences*, vol. 58, pp. 191–207, 2017.

[4] P. S. M. Dunlop, M. Ciavola, L. Rizzo, D. A. McDowell, and J. A. Byrne, "Effect of photocatalysis on the transfer of antibiotic resistance genes in urban wastewater," *Catalysis Today*, vol. 240, pp. 55–60, 2015.

[5] N. D. Friedman, E. Temkin, and Y. Carmeli, "The negative impact of antibiotic resistance," *Clinical Microbiology and Infection*, vol. 22, no. 5, pp. 416–422, 2016.

[6] R. Nosrati, A. Olad, and S. Shakoori, "Preparation of an antibacterial, hydrophilic and photocatalytically active polyacrylic coating using TiO_2 nanoparticles sensitized by graphene oxide," *Materials Science and Engineering: C*, vol. 80, pp. 642–651, 2017.

[7] B. Liu, L. Mu, B. Han, J. Zhang, and H. Shi, "Fabrication of TiO_2/Ag_2O heterostructure with enhanced photocatalytic and antibacterial activities under visible light irradiation," *Applied Surface Science*, vol. 396, pp. 1596–1603, 2017.

[8] D. M. Tobaldi, C. Piccirillo, N. Rozman et al., "Effects of Cu, Zn and Cu-Zn addition on the microstructure and antibacterial and photocatalytic functional properties of Cu-Zn modified TiO_2 nano-heterostructures," *Journal of Photochemistry and Photobiology A: Chemistry*, vol. 330, pp. 44–54, 2016.

[9] R. Ahmad, Z. Ahmad, A. U. Khan, N. R. Mastoi, M. Aslam, and J. Kim, "Photocatalytic systems as an advanced environmental remediation: recent developments, limitations and new avenues for applications," *Journal of Environmental Chemical Engineering*, vol. 4, no. 4, pp. 4143–4164, 2016.

[10] C. Adán, J. Marugán, S. Mesones, C. Casado, and R. van Grieken, "Bacterial inactivation and degradation of organic molecules by titanium dioxide supported on porous stainless steel photocatalytic membranes," *Chemical Engineering Journal*, vol. 318, pp. 29–38, 2017.

[11] S. K. Misra, S. I. Andronenko, D. Tipikin, J. H. Freed, V. Somani, and O. Prakash, "Study of paramagnetic defect centers in as-grown and annealed TiO_2 anatase and rutile nanoparticles by a variable-temperature X-band and high-frequency (236 GHz) EPR," *Journal of Magnetism and Magnetic Materials*, vol. 401, pp. 495–505, 2016.

[12] J. Wang, W. Liu, H. Li et al., "Preparation of cellulose fiber–TiO_2 nanobelt–silver nanoparticle hierarchically structured hybrid paper and its photocatalytic and antibacterial properties," *Chemical Engineering Journal*, vol. 228, pp. 272–280, 2013.

[13] J. Singh, S. A. Khan, J. Shah, R. K. Kotnala, and S. Mohapatra, "Nanostructured TiO_2 thin films prepared by RF magnetron sputtering for photocatalytic applications," *Applied Surface Science*, vol. 422, pp. 953–961, 2017.

[14] M. R. Eskandarian, H. Choi, M. Fazli, and M. H. Rasoulifard, "Effect of UV-LED wavelengths on direct photolytic and TiO_2 photocatalytic degradation of emerging contaminants in water," *Chemical Engineering Journal*, vol. 300, pp. 414–422, 2016.

[15] L. C. Ferreira, M. S. Lucas, J. R. Fernandes, and P. B. Tavares, "Photocatalytic oxidation of Reactive Black 5 with UV-A LEDs," *Journal of Environmental Chemical Engineering*, vol. 4, no. 1, pp. 109–114, 2016.

[16] T. Rojviroon, O. Rojviroon, and S. Sirivithayapakorn, "Photocatalytic decolourisation of dyes using TiO_2 thin film photocatalysts," *Surface Engineering*, vol. 32, no. 8, pp. 562–569, 2016.

[17] W. Su, S. S. Wei, S. Q. Hu, and J. X. Tang, "Preparation of TiO_2/Ag colloids with ultraviolet resistance and antibacterial property using short chain polyethylene glycol," *Journal of Hazardous Materials*, vol. 172, no. 2-3, pp. 716–720, 2009.

[18] S. Guo, R. Huang, and H. Chen, "Application of water-assisted ultraviolet light in combination of chlorine and hydrogen peroxide to inactivate *Salmonella* on fresh produce," *International Journal of Food Microbiology*, vol. 257, pp. 101–109, 2017.

[19] J. F. Guayaquil-Sosa, B. Serrano-Rosales, P. J. Valadés-Pelayo, and H. de Lasa, "Photocatalytic hydrogen production using mesoporous TiO_2 doped with Pt," *Applied Catalysis B: Environmental*, vol. 211, pp. 337–348, 2017.

[20] C. Dette, M. A. Pérez-Osorio, C. S. Kley et al., "TiO_2 anatase with a bandgap in the visible region," *Nano Letters*, vol. 14, no. 11, pp. 6533–6538, 2014.

[21] G. Pathak, S. Pandey, R. Katiyar et al., "Analysis of photoluminescence, UV absorbance, optical band gap and threshold voltage of TiO_2 nanoparticles dispersed in high birefringence nematic liquid crystal towards its application in display and photovoltaic devices," *Journal of Luminescence*, vol. 192, pp. 33–39, 2017.

[22] D.-J. Huang and T.-S. Leu, "Fabrication of high wettability gradient on copper substrate," *Applied Surface Science*, vol. 280, pp. 25–32, 2013.

[23] J. C. Joud, M. Houmard, and G. Berthomé, "Surface charges of oxides and wettability: application to TiO_2–SiO_2 composite films," *Applied Surface Science*, vol. 287, pp. 37–45, 2013.

[24] M. Alzamani, A. Shokuhfar, E. Eghdam, and S. Mastali, "Influence of catalyst on structural and morphological properties of TiO_2 nanostructured films prepared by sol–gel on glass," *Progress in Natural Science: Materials International*, vol. 23, no. 1, pp. 77–84, 2013.

[25] J. Du, Q. Wu, S. Zhong et al., "Effect of hydroxyl groups on hydrophilic and photocatalytic activities of rare earth doped titanium dioxide thin films," *Journal of Rare Earths*, vol. 33, no. 2, pp. 148–153, 2015.

[26] D. Luca, D. Mardare, F. Iacomi, and C. M. Teodorescu, "Increasing surface hydrophilicity of titania thin films by doping," *Applied Surface Science*, vol. 252, no. 18, pp. 6122–6126, 2006.

[27] L. Huang, S. Jing, O. Zhuo, X. Meng, and X. Wang, "Surface hydrophilicity and antifungal properties of TiO_2 films coated on a Co-Cr substrate," *BioMed Research International*, vol. 2017, Article ID 2054723, 7 pages, 2017.

[28] F. Li, Q. Li, and H. Kim, "Spray deposition of electrospun TiO_2 nanoparticles with self-cleaning and transparent properties onto glass," *Applied Surface Science*, vol. 276, pp. 390–396, 2013.

[29] B. Yu, K. M. Leung, Q. Guo, W. M. Lau, and J. Yang, "Synthesis of Ag-TiO_2 composite nano thin film for antimicrobial application," *Nanotechnology*, vol. 22, no. 11, article 115603, 2011.

[30] T. Rojviroon and S. Sirivithayapakorn, "Properties of TiO_2 thin films prepared using sol–gel process," *Surface Engineering*, vol. 29, no. 1, pp. 77–80, 2013.

[31] S. Vyas, R. Tiwary, K. Shubham, and P. Chakrabarti, "Study the target effect on the structural, surface and optical properties of TiO_2 thin film fabricated by RF sputtering method," *Superlattices and Microstructures*, vol. 80, pp. 215–221, 2015.

[32] B. R. Cruz-Ortiz, J. W. J. Hamilton, C. Pablos et al., "Mechanism of photocatalytic disinfection using titania-graphene composites under UV and visible irradiation," *Chemical Engineering Journal*, vol. 316, pp. 179–186, 2017.

[33] J. Zhang and Y. Nosaka, "Mechanism of the OH radical generation in photocatalysis with TiO_2 of different crystalline types," *The Journal of Physical Chemistry C*, vol. 118, no. 20, pp. 10824–10832, 2014.

[34] J. Zheng, C. Su, J. Zhou, L. Xu, Y. Qian, and H. Chen, "Effects and mechanisms of ultraviolet, chlorination, and ozone disinfection on antibiotic resistance genes in secondary effluents of municipal wastewater treatment plants," *Chemical Engineering Journal*, vol. 317, pp. 309–316, 2017.

[35] X. Huang, Y. Qu, C. A. Cid et al., "Electrochemical disinfection of toilet wastewater using wastewater electrolysis cell," *Water Research*, vol. 92, pp. 164–172, 2016.

[36] B. Sun, M. Sato, and J. Sid Clements, "Optical study of active species produced by a pulsed streamer corona discharge in water," *Journal of Electrostatics*, vol. 39, no. 3, pp. 189–202, 1997.

[37] J. J. Murcia, E. G. Ávila-Martínez, H. Rojas, J. A. Navío, and M. C. Hidalgo, "Study of the *E. coli* elimination from urban wastewater over photocatalysts based on metallized TiO_2," *Applied Catalysis B: Environmental*, vol. 200, pp. 469–476, 2017.

[38] D. Sethi and R. Sakthivel, "ZnO/TiO_2 composites for photocatalytic inactivation of *Escherichia coli*," *Journal of Photochemistry and Photobiology B: Biology*, vol. 168, pp. 117–123, 2017.

[39] V. Binas, D. Venieri, D. Kotzias, and G. Kiriakidis, "Modified TiO_2 based photocatalysts for improved air and health quality," *Journal of Materiomics*, vol. 3, no. 1, pp. 3–16, 2017.

[40] J. Mac Mahon, S. C. Pillai, J. M. Kelly, and L. W. Gill, "Solar photocatalytic disinfection of *E. coli* and bacteriophages MS2, ΦX174 and PR772 using TiO_2, ZnO and ruthenium based complexes in a continuous flow system," *Journal of Photochemistry and Photobiology B: Biology*, vol. 170, pp. 79–90, 2017.

[41] J. Ma, C. Zhu, J. Lu et al., "Catalytic degradation of gaseous benzene by using TiO_2/goethite immobilized on palygorskite: preparation, characterization and mechanism," *Solid State Sciences*, vol. 49, pp. 1–9, 2015.

[42] N. R. Khalid, A. Majid, M. B. Tahir, N. A. Niaz, and S. Khalid, "Carbonaceous-TiO_2 nanomaterials for photocatalytic degradation of pollutants: a review," *Ceramics International*, vol. 43, no. 17, pp. 14552–14571, 2017.

[43] J. Ø. Hansen, R. Bebensee, U. Martinez et al., "Unravelling site-specific photo-reactions of ethanol on rutile $TiO_2(110)$," *Scientific Reports*, vol. 6, no. 1, article 21990, 2016.

[44] R. van Grieken, J. Marugán, C. Pablos, L. Furones, and A. López, "Comparison between the photocatalytic inactivation of Gram-positive *E. faecalis* and Gram-negative *E. coli* faecal contamination indicator microorganisms," *Applied Catalysis B: Environmental*, vol. 100, no. 1-2, pp. 212–220, 2010.

[45] T.-D. Pham and B.-K. Lee, "Effects of Ag doping on the photocatalytic disinfection of *E. coli* in bioaerosol by Ag–TiO_2/GF under visible light," *Journal of Colloid and Interface Science*, vol. 428, pp. 24–31, 2014.